

Energy Management and Control of a Flywheel Storage System for Peak Shaving Applications

Lysandros Tziouvani, *Student Member, IEEE*, Lenos Hadjidemetriou, *Member, IEEE*, Charalampos Charalampous, Maria Tziakouri, Stelios Timotheou, *Senior Member, IEEE*, Elias Kyriakides, *Senior Member, IEEE*

Dedicated to the memory of Elias Kyriakides.

Abstract—Peak shaving applications provided by energy storage systems enhance the utilization of existing grid infrastructure to accommodate the increased penetration of renewable energy sources. This work investigates the provision of peak shaving services from a flywheel energy storage system installed in a transformer substation. A lexicographic optimization scheme is formulated to define the flywheel power set-points by minimizing the transformer power limit violations and the flywheel energy losses. Convex functions that represent the flywheel power losses and its maximum power are derived and integrated in the proposed scheme. A two-level hierarchical control framework is introduced to operate the transformer-flywheel-system in a way that handles prediction errors and modelling inaccuracies. At the higher level, a model predictive controller is developed that solves the lexicographic optimization scheme using linear programming. At the lower-level, a secondary controller corrects the power set-points of the model predictive controller using real-time measurements. A software platform has been developed for integrating the proposed controllers in an experimental setup to test their effectiveness in a realistic testbed setting, and the flywheel system characteristics are experimentally identified. Simulation and experimental results validate and verify the modelling, identification, control and operation of a real flywheel system for peak shaving services.

Index Terms—Active distribution grids, FIWARE, flywheel energy storage system, lexicographic optimization, model predictive control, peak shaving services, secondary control.

I. INTRODUCTION

THE increasing penetration of Photovoltaic (PV) generation into the distribution grid along with the load demand growth can cause reverse and direct power flow violations in distribution transformers. As a result, the distribution grids can operate outside of their safely limits, particularly in cases with extensive integration of PVs and electric vehicle charging stations. Nevertheless, the safe and reliable operation of distribution grids can be maintained by energy storage systems

This work was supported by the European Regional Development Fund and the Republic of Cyprus through the Research and Innovation Foundation (Project: INTEGRATED/0916/0035 - EMPOWER). It was also partially supported by the European Union's Horizon 2020 research and innovation programme under grant agreement No 957739 (OneNet), by the European Union's Horizon 2020 research and innovation programme under grant agreement No 739551 (KIOS CoE) and from the Government of the Republic of Cyprus through the Directorate General for European Programmes, Coordination and Development.

L. Tziouvani, L. Hadjidemetriou, C. Charalampous, M. Tziakouri and S. Timotheou are with KIOS Research and Innovation Center of Excellence and the Department of Electrical and Computer Engineering, University of Cyprus, 1678 Nicosia, Cyprus (e-mail: {ltziouv01, lhadjji02, cchara63, mtziak01, stimo}@ucy.ac.cy).

E. Kyriakides, deceased, was with the KIOS Research and Innovation Center of Excellence and the Department of Electrical and Computer Engineering, University of Cyprus, 1678 Nicosia, Cyprus.

(ESSs) that provide peak shaving services [1]. ESSs enhance the capacity of existing distribution grids to accommodate the load and PV generation growth in order to avoid any violations of the maximum power limit of the distribution transformers [2]. Towards this direction, this work develops an energy management and control scheme for a flywheel energy storage system (FESS) to provide peak shaving services to the distribution grid. Among the different types of ESSs, FESSs are suitable for applications that require short-time power quality services and peak-load regulation, since they are characterized by full depth discharge capability, 85-90% efficiency rate, very long lifetime, environmental friendliness, lower maintenance cost and high charging-discharging abilities compared to battery energy storage systems (BESS) [3].

Peak shaving applications are investigated in [4]-[5] for planning purposes, to examine the location, sizing and cost-benefit of the ESSs. In addition, peak shaving services provided to distribution grids using BESSs are proposed in [6]-[11] for operational purposes using optimization methods. These services are provided by minimizing the daily peak power [6]-[9] or the square of the power drawn from the feeder [10]. Also, in [8] and [9] predicted load uncertainties are addressed using stochastic formulations. Note that weighted multi-objective functions are used in [8]-[10] where a first objective is associated with peak shaving and a second objective with the health and longevity of a BESS. In these formulations, an improvement in the first objective can deteriorate the second objective; however, the optimal trade-off between the conflicting objectives has not been considered. The BESS health objective can be ignored when using a FESS, because FESSs have very high number of cycles and high charging/discharging rate.

A peak shaving application using a FESS is presented in [12] to reduce the maximum power demand of shore-to-ship cranes. Power smoothing applications in wind power plants using FESSs are presented in [13]-[14]. These are short-time applications that smooth the power injected to the grid and compensate power disturbances. Note that FESSs are not suitable for long term energy storage because they suffer from high standby losses, as the self-discharge can reach 20% per hour [3]. However, hybrid wind-FESS energy management schemes are presented in [15]-[16] to compensate the main drawback of the FESSs by formulating optimization schemes that minimize the FESS standby losses. Specifically, a model predictive controller and a secondary real-time controller are used in [16], to shift the surplus wind energy and to compensate the wind-power prediction error. The aforementioned works control a FESS using models that are dependent on

technical characteristics such as the angular speed and the stator current and voltage. Nevertheless, these characteristics are not always available through commercial FESS interfaces. The available measurements in commercial interfaces are the State-of-Charge (SoC) and the instant charging/discharging rate, while users can command the FESS to maintain a constant charging/discharging power or SoC. In addition, the associated FESS models can lead to non-convex optimization problems which are challenging to solve [15].

This work aims to eliminate the power violations of a distribution transformer using a FESS and minimize the FESS power losses for a cost-effective operation of the distribution grid. A novel lexicographic optimization scheme is formulated that derives the FESS power set-points to minimize the transformer power limit violations and the FESS energy losses. Functions that represent the power losses and maximum power of a FESS are derived and integrated in the proposed scheme. In detail, two linear functions that model the FESS power losses based on the charging mode are derived as a function of the charging/discharging power and the SoC. Also, a nonlinear function is derived to associate the FESS maximum charging/discharging power with the SoC due to the rated current limit imposed by the power electronics converter.

A two-level hierarchical control scheme is proposed that minimizes the objectives of the lexicographic optimization problem and deals with demand prediction errors and modelling uncertainties. At the higher-level, a model predictive controller is developed that handles the considered problem by sequentially solving four linear optimization problems. At the lower-level, a secondary controller corrects the control signals using real-time measurements at a shorter time-scale.

The proposed hierarchical control scheme is integrated and validated in an experimental setup. Towards this direction, a software platform based on FIWARE [17] has been developed that enables the monitoring and control of a flywheel system in a smart grid environment. Model validation and parameter identification is experimentally performed for the prototype FESS, indicating the high accuracy of the derived functions to estimate the FESS power losses and maximum power. In addition, simulation and experimental results validate the effectiveness of the proposed energy management and control scheme to provide peak shaving services, enabling the active management of smart distribution grids. In summary, this work has four main contributions.

- 1) FESS power losses and maximum power functions are constructed to be dependent on parameters that are readily available through commercial FESS interfaces (charging/discharging power and SoC). Moreover, the derived FESS functions are modelled with convex constraints that enable the formulation of convex optimization problems.
- 2) The derived FESS functions are used to develop a new optimization formulation for the peak-shaving problem that minimizes the transformer power limit violations and FESS power losses in a lexicographic fashion.
- 3) A two-level hierarchical control scheme is developed to solve the peak-shaving problem fast and reliably, while handling prediction errors and modelling inaccuracies.
- 4) A software platform is developed for managing smart grid

configurations and utilized for the integration of a prototype FESS system into a smart-grid testbed used for the experimental evaluation of the proposed control scheme. In addition, model validation and parameter identification is experimentally performed for the prototype FESS.

The remainder of this paper is organized as follows. Section II explains the concept of lexicographic optimization. Section III states the problem and Section IV models the maximum power and power losses of a FESS. The two-level hierarchical solution methodology is then described in Section V. The proposed solution methodology is evaluated both in simulation and experimentally in Sections VI and VII, respectively. Finally, Section IX concludes the paper.

II. PRELIMINARIES - LEXICOGRAPHIC OPTIMIZATION

In lexicographic optimization L objective functions, $\psi_l(\mathbf{x})$ $l = 1, \dots, L$, are to be optimized on a feasible set $\mathbf{x} \in \mathcal{X}$ in a *lexicographic order* such that $\psi_l(\mathbf{x})$ has higher priority than $\psi_{l+1}(\mathbf{x})$ [18]. This means that low priority objectives are optimized as far as they do not affect the optimization of higher priority objectives. Let us denote the L -objective lexicographic optimization problem by

$$\begin{aligned} \text{lexmin } \{ \psi_1(\mathbf{x}), \psi_2(\mathbf{x}), \dots, \psi_L(\mathbf{x}) \} \\ \text{s.t. } \mathbf{x} \in \mathcal{X}. \end{aligned} \quad (1)$$

Optimizing problem (1) requires the solution of L optimization subproblems with the l -th one defined as

$$\min \psi_l(\mathbf{x}) \quad (2)$$

$$\begin{aligned} \text{s.t. } \psi_m(\mathbf{x}) \leq \psi_m(\mathbf{x}_m^*), \quad m = 1, \dots, l-1, \\ \mathbf{x} \in \mathcal{X}, \end{aligned} \quad (3)$$

where \mathbf{x}_m^* denotes the optimal solution of the m -th subproblem. Then, the optimal solution to problem (1) is \mathbf{x}_L^* .

III. PROBLEM STATEMENT

This work considers the provision of peak shaving services to a medium voltage/low voltage (MV/LV) transformer substation. At the LV side, the substation bus with an installed FESS is connected to an LV distribution grid with consumer and PV installations, as illustrated in Fig. 1. Peak shaving is achieved by managing the FESS power set-points to minimize in a lexicographic fashion: (i) the transformer peak power violation, (ii) the transformer energy violation, (iii) the SoC energy violations to sustain a minimum desirable SoC in the FESS and (iv) the FESS power losses. The considered problem, denoted by \mathbb{P}_{LEX} , is given by

$$\text{lexmin } \{ f_V(\mathbf{x}), f_E(\mathbf{x}), f_U(\mathbf{w}), f_L(\mathbf{P}^L) \} \quad (\mathbb{P}_{LEX}) \quad (4a)$$

$$\text{s.t. } \underline{P}^F - x_t \leq P_t^F \leq \overline{P}^F + x_t, \quad \forall t \in \mathcal{T}, \quad (4b)$$

$$C_t^S + w_t \geq \underline{C}_t^d, \quad \forall t \in \mathcal{T}, \quad (4c)$$

$$P_t^F + P_t^S = D_t^A, \quad \forall t \in \mathcal{T}, \quad (4d)$$

$$C_{t+1}^S = C_t^S + \Delta T(-P_t^S - P_t^L), \quad \forall t \in \mathcal{T}, \quad (4e)$$

$$C_0^S = I^c, \quad 0 \leq C_t^S \leq \overline{C}^S, \quad \forall t \in \mathcal{T}, \quad (4f)$$

$$\underline{P}^S \leq P_t^S \leq \overline{P}^S, \quad \forall t \in \mathcal{T}, \quad (4g)$$

$$|P_t^S| \leq g(C_t^S), \quad \forall t \in \mathcal{T}, \quad (4h)$$

$$P_t^L \geq h(C_t^S, P_t^S), \quad \forall t \in \mathcal{T}, \quad (4i)$$

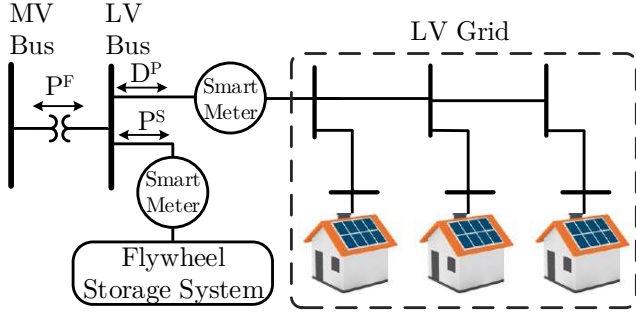


Fig. 1. Peak shaving services to a LV distribution grid.

where $\mathcal{T} = \{1, \dots, T/\Delta T\}$, T is the time-horizon and ΔT is the time-step duration considered.

In problem \mathbb{P}_{LEX} , variable P_t^F denote the transformer power, P_t^S the FESS charging (negative values) and discharging power (positive values), P_t^L the FESS power losses, x_t the transformer maximum power violation, while C_t^S and w_t denote the SoC and the SoC energy violation of the FESS at time t , respectively. \mathbf{P}^L , \mathbf{x} and \mathbf{w} are vector forms of P_t^L , x_t and w_t , $\forall t \in \mathcal{T}$, respectively; for example, $\mathbf{x} = [x_1, \dots, x_t, \dots, x_T]$. Parameters \underline{P}^F [\overline{P}^F] and \underline{P}^S [\overline{P}^S] denote the minimum [maximum] transformer and FESS power, respectively, \overline{C}^S the maximum SoC, while I^c denotes the initial FESS state. Parameter D_t^A is the actual net load demand of the LV grid defined as

$$D_t^A = D_t^P + \xi_t, \quad \forall t \in \mathcal{T}, \quad (5)$$

where D_t^P is the predicted net load of the LV grid and ξ_t is the prediction error at time-step t . D_t^A is generally unknown; hence, the predicted load is used in practical applications.

The first objective of \mathbb{P}_{LEX} is to minimize a function $f_V(\mathbf{x})$ of transformer maximum power violations, while the second objective, $f_E(\mathbf{x})$, is to minimize the transformer energy violations. To achieve this, soft constraint (4b) is introduced to restrain the transformer power within its limit; variables x_t obtain non-zero values when transformer power limit violations are unavoidable. The third objective is to minimize the SoC energy violations, $f_U(\mathbf{w})$, to sustain a minimum desirable SoC in the FESS, \underline{C}_t^d , according to soft constraint (4c). This minimum SoC of the FESS is used in Section V to address the transformer power limit violations that are caused by the load demand uncertainty. The fourth objective is to minimize the FESS power losses $f_L(\mathbf{P}^L)$. Note that low priority objectives are optimized as far as they do not affect the optimal solution of higher priority objectives. In Section V, the four objectives are mathematically defined and the reasons for the selected lexicographic order are explained.

In addition to constraints (4b) and (4c) which relate to the objectives of \mathbb{P}_{LEX} , the problem includes six more constraints. The power balance equation (4d) aims to select the FESS charging/discharging power to compensate for load demand exceeding the transformer maximum power to avoid transformer power limit violations. The FESS SoC dynamic state equations are defined in (4e) - (4f) and the charging/discharging power limits in (4g). Eq. (4e) takes into consideration the FESS power losses defined in (4i). Finally, Eq. (4h) restricts the maximum charging/discharging power as a function of the SoC.

Problem \mathbb{P}_{LEX} is convex when functions $f_V(\mathbf{x})$, $f_E(\mathbf{x})$, $f_U(\mathbf{w})$, $f_L(\mathbf{P}^L)$ and $h(C_t^S, P_t^S)$ are convex and function $g(C_t^S)$ is concave. Section IV details the modelling and derivation of standard-form convex expressions of the FESS functions $g(C_t^S)$ and $h(C_t^S, P_t^S)$ that appear in Eqs. (4h) and (4i), respectively. Then, Section V proposes a two-level hierarchical control scheme to handle Problem \mathbb{P}_{LEX} under demand uncertainty.

IV. FESS MODELLING

A. FESS Power Losses

A FESS is a kinetic energy storage technology composed of mechanical components, an electrical machine and a power converter. The stored energy in kinetic form is given by

$$C^S(t) = 0.5J\omega_r^2(t), \quad \forall t \in \mathcal{T}, \quad \Rightarrow \quad C^S \sim \omega_r^2, \quad (6)$$

where J is the moment of inertia and ω_r is the angular speed [3]. Notice that the stored energy is analogous to ω_r^2 . Power losses occur at all components depending on the operational condition of a FESS. Specifically, windage and bearing friction losses occur in the mechanical components; hysteresis losses, eddy currents and copper losses occur in the electrical machine; conduction and switching losses occur in the power electronics converter [19]. The windage and eddy currents losses are proportional to ω_r^2 ; while bearing and hysteresis losses are proportional to ω_r [19]. Therefore, the power losses in a FESS are usually described by polynomial functions of ω_r , such as $c_1\omega_r^2$ [20], and $c_1\omega_r^2 + c_2\omega_r$ [15]-[16], [19], where c_1 and c_2 are constants. A more accurate representation considers different FESS power losses functions for the charging and discharging modes [21].

In this work, two linear functions are proposed to represent the FESS power losses based on the charging mode. The power losses of each mode are described by a linear function of the charging/discharging power and the SoC as shown in Table I. In Eqs. (7b) and (7c), P_t^d and P_t^c denote the power losses of the discharging and charging mode, respectively, while \hat{b}^c , \hat{b}^d , \hat{c}^c and \hat{c}^d are positive constants depended on the FESS structure and characteristics. In the proposed representation, term C^S corresponds to ω_r^2 according to (6); thus, the terms $\hat{c}^d C_t^S$ and $\hat{c}^c C_t^S$ represent the polynomial term $c_1\omega_r^2$. Note that $c_1\omega_r^2$ is the dominant power losses term of the polynomial function $c_1\omega_r^2 + c_2\omega_r$, especially at high speeds and with reduced bearing friction losses (since low-friction magnetic bearings are typically used in flywheel applications) [19], [22]-[23]. In addition, the terms $\hat{b}^d P_t^d$ and $\hat{b}^c P_t^c$ consider the FESS power losses for the charging and discharging modes. Logical constraints in (7a) and (7d) are introduced to select the appropriate function based on the charging mode. The power losses parameters in Eqs. (7b) - (7c) can be experimentally estimated for any real FESS system using the proposed methodology presented in Section VII-B. Moreover, when the round-trip efficiency, e^r , and the standby losses per hour, l^s , of a commercial FESS are given by the manufacturer datasheet, e.g. $e^r = 85\%$ and $l^s = 20\%$ [3], then the FESS power losses can be represented using Eqs. (7b) - (7c) by setting $\hat{b}^c = \hat{b}^d = (100\% - e^r)/2$ and $\hat{c}^c = \hat{c}^d = l^s$.

Incorporating Eqs. (7a) - (7d) into Problem \mathbb{P}_{LEX} leads to non-convex optimization formulations due to the presence of

TABLE I
FESS POWER LOSSES AND FESS MAXIMUM POWER LIMIT

Derived Constraints		Convex Affine Constraints	
$P_t^L = \delta P_t^d + (1 - \delta)P_t^c$	(7a)	$P_t^L \geq \hat{b}^d P_t^S + \hat{c}^d C_t^S, \forall t \in \mathcal{T}$	(8a)
$P_t^d = \hat{b}^d P_t^S + \hat{c}^d C_t^S$	(7b)	$P_t^L \geq -\hat{b}^c P_t^S + \hat{c}^c C_t^S, \forall t \in \mathcal{T}$	(8b)
$P_t^c = -\hat{b}^c P_t^S + \hat{c}^c C_t^S$	(7c)	$P_t^S \leq \alpha_i + \beta_i C_t^S, \forall t, \forall i \in \mathcal{N}$	(8c)
$\delta_t = \begin{cases} 1, & P_t^S \geq 0 \\ 0, & P_t^S < 0 \end{cases}$	(7d)	$P_t^S \geq -\alpha_i - \beta_i C_t^S, \forall t, \forall i \in \mathcal{N}$	(8d)
$ P_t^S \leq \hat{\alpha} + \hat{\beta} \sqrt{C_t^S}$	(7e)		

binary variables. To avoid this issue, notice that when $P_t^S \geq 0$ it is true that $P_t^d \geq P_t^c$ since $\hat{b}^c, \hat{b}^d, \hat{c}^c, \hat{c}^d$ and C_t^S are positive; conversely, when $P_t^S \leq 0$ it is true that $P_t^c \geq P_t^d$. These imply that $h(C_t^S, P_t^S) = \max\{P_t^d, P_t^c\}$. Hence, constraint (4i) is convex and can be equivalently represented by affine constraints (8a) and (8b). Constraints (8a) and (8b) are binding when $P_t^S \geq 0$ and $P_t^S \leq 0$, respectively.

The derived functions of the FESS power losses enable:

- 1) Accurate approximation of the FESS losses, capturing the dominant losses term $c_1 \omega_r^2$ and the power losses from the charging/discharging modes. The high accuracy of the approximated FESS losses is experimentally validated for a real prototype FESS in Section VII-B.
- 2) Easy integration of commercial FESSs in practical applications because the FESS power losses are dependent on the SoC and charging/discharging power, independent of ω_r and J , which are readily available through a FESS interface.
- 3) Effective incorporation into mathematical programs as linear constraints that can be efficiently handled by appropriate optimization tools.

B. FESS Maximum Power

Constraint (7e) aims to restrict the maximum charging/discharging power through function $g(C_t^S)$. The dependence on C_t^S is explained below. The maximum charging/discharging power of a FESS system depends on the rated current limit (\hat{I}) of the machine side power electronics converter. For given \hat{I} , the rated converter power \hat{P} is directly related to the stator voltage V of the FESS electrical machine [24], and expressed as

$$\hat{P}(t) = 3V(t)\hat{I}, \quad \forall t \in \mathcal{T}, \quad \Rightarrow \quad \hat{P} \sim V. \quad (9)$$

In permanent magnet synchronous machines (widely used in FESS applications), the stator voltage is directly related to the angular speed, given a constant magnetic flux, and given by

$$V(t) = K\Phi\omega_r(t), \quad \forall t \in \mathcal{T}, \quad \Rightarrow \quad V \sim \omega_r, \quad (10)$$

where K is a machine constant and Φ is the magnetic flux. Thus, V is directly related to ω_r such that $\hat{P} \sim \omega_r$ [25]. Since $C^S \sim \omega_r^2$, according to Eq. (6), it can be concluded that the maximum power is directly related to the square root of the SoC, i.e., $\hat{P} \sim \sqrt{C^S}$. Hence, we consider that $g(C_t^S) = \hat{\alpha} + \hat{\beta}\sqrt{C_t^S}$, where $\hat{\alpha}$ and $\hat{\beta}$ are positive constants, such that the maximum FESS power is constrained by (7e). The constants $\hat{\alpha}$ and $\hat{\beta}$ can be identified using linear regression either directly based on the maximum power curve provided

in the FESS datasheet, or indirectly through measurements obtained from the FESS interface as presented in Section VII-B. Function $g(C_t^S)$ is monotonically increasing and concave, such that Eq. (7e) is convex. To avoid the introduction of general convex constraints in Problem \mathbb{P}_{LEX} , a piecewise linear approximation with N segments is constructed for $g(C_t^S)$. Let the i -th linear segment be $\alpha_i + \beta_i C_t^S, \forall i \in \mathcal{N} = \{1, \dots, N\}$. Then, the affine constraints (8c)-(8d) provide the maximum values for $|P_t^S|$.

V. SOLUTION METHODOLOGY

This section presents the proposed methodology for the solution of the peak shaving problem under demand prediction errors, described in Section III.

A. Control Architecture

To deal with demand prediction errors, a two-level hierarchical control architecture is proposed, as shown in Fig. 2. At the higher level, a model predictive controller (tertiary level control) optimizes the FESS power set-points, P_t^S , over a moving time horizon, \mathcal{T} , based on the transformer predicted net load demand, D_t^P , and the measured FESS SoC, I^c . At the lower level, a secondary controller (SC) compensates the net load prediction error by revising the FESS set-points at a shorter time-scale. A primary controller is embedded in the FESS (in the plant) that drives the power converters to regulate FESS operation in real time.

The time sequence of events of the considered control architecture is depicted in Fig. 3. The MPC control step duration is set to T_{MPC} . Measurements are collected every T_m time-units for system monitoring and used as input to the controllers. The MPC controller solves Problem \mathcal{P}_{LEX} , using the latest SoC measurement, at the end of every MPC control-step, aiming to define the next FESS power set-point. The SC controller updates the MPC-defined FESS set-point every T_{SC} time-units using the latest load measurement.

In multi-level control architectures, the inner loop needs to be significantly faster than the outer loop, $T_{MPC} > T_{SC}$, to decouple the dynamics between the two controllers. In addition, the maximum execution time needed for the solution of the MPC problem, T_{ex} , should be smaller than the MPC control-step such that $T_{MPC} > T_{ex}$. For monitoring both the dynamic and steady state operation of the FESS, measurements with higher sampling rate are required, yielding $T_m < T_{SC} < T_{MPC}$.

B. Model Predictive Controller

The MPC controller elaborates on the definition of Problem \mathbb{P}_{LEX} to define a convex lexicographic optimization problem with four objectives. The first and second objectives minimize the transformer maximum power and energy violations, respectively, based on the predicted load. The third objective aims to sustain a minimum desirable SoC in the FESS that can be used by the SC controller to compensate the transformer power violations due to the load uncertainty. Therefore, the third objective minimizes the SoC energy violations. The fourth objective minimizes the FESS energy losses. This lexicographic order gives first priority to the transformer safety; thus, the first and second objectives minimize the

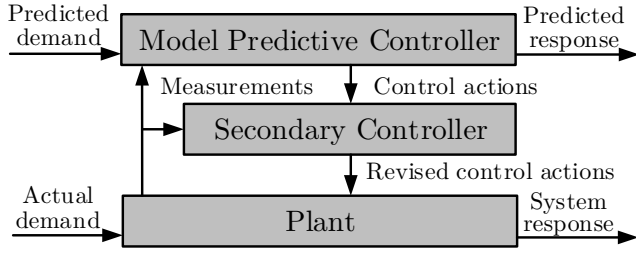


Fig. 2. Hierarchical level control architecture.

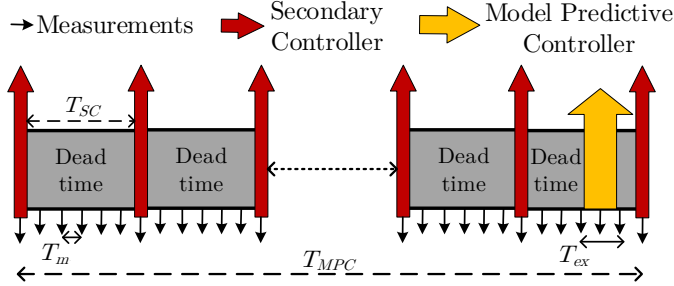


Fig. 3. Time sequence of events in each cycle of the MPC framework.

“expected” violations. The third objective aims to address “unexpected” violations. Last, the cost-effective operation is achieved by minimizing the FESS losses. According to the general principles of lexicographic optimization outlined in Section II, the 4-objective Problem \mathbb{P}_{LEX} can be solved by sequentially solving four single-objective problems, \mathbb{P}_V , \mathbb{P}_E , \mathbb{P}_U and \mathbb{P}_L , associated with objectives $f_V(\mathbf{x})$, $f_E(\mathbf{x})$, $f_U(\mathbf{w})$ and $f_L(\mathbf{P}^L)$, respectively.

Problem \mathbb{P}_V aims to eliminate the transformer power limit violations by minimizing the peak power violation of the transformer defined as $f_V(\mathbf{x}) = \max_{t \in \mathcal{T}} x_t$. Towards this direction, Problem \mathbb{P}_V is defined as:

$$\min_{\mathbf{x}} f_V(\mathbf{x}) = \max_{t \in \mathcal{T}} \{x_t\} \quad (\mathbb{P}_V) \quad (11a)$$

$$\text{s.t. Constraints (4b), (4e)-(4g), (8a)-(8d),} \quad (11b)$$

$$P_t^F + P_t^S = D_t^P, \quad \forall t \in \mathcal{T}. \quad (11c)$$

Eq. (11c) has been used instead of (4d) because the actual demand is unknown. Problem \mathbb{P}_V can be converted into a linear program by transforming the objective as: $\{\text{minimize } z, \text{ s.t. } 0 \leq x_t \leq z, \forall t \in \mathcal{T}\}$.

Let x_t^V denote the optimal values of $x_t, \forall t \in \mathcal{T}$, derived from the solution of Problem \mathbb{P}_V . Then, Problem \mathbb{P}_E aims to minimize the total energy violations of the transformer yielding the formulation

$$\min_{\mathbf{x}} f_E(\mathbf{x}) = \sum_{t \in \mathcal{T}} x_t \Delta T \quad (\mathbb{P}_E) \quad (12a)$$

$$\text{s.t. Constraints (4b), (4e)-(4g), (8a)-(8d), (11c),} \quad (12b)$$

$$0 \leq x_t \leq \max_{t \in \mathcal{T}} \{x_t^V\}, \quad \forall t \in \mathcal{T}. \quad (12c)$$

Note that there is no need to solve Problem \mathbb{P}_E when $\max_{t \in \mathcal{T}} \{x_t^V\} = 0$ because there are no transformer power limit violations. Simulation results in Section VI-A indicate that the combination of the first and second objectives, $f_V(\mathbf{x})$ and $f_E(\mathbf{x})$, in this lexicographic order provides better results compared to the case that only one objective is used.

Problem \mathbb{P}_U aims to handle demand prediction uncertainty by minimizing the SoC energy violations, w_t , to sustain a

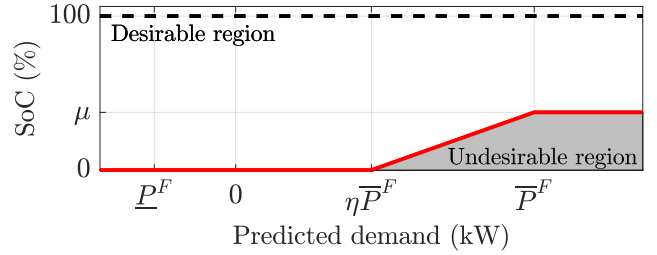


Fig. 4. Minimum Desirable FESS SoC as a function of the predicted demand.

minimum desirable SoC, \underline{C}_t^d , according to Eq. (4c). Parameter \underline{C}_t^d is a function of the predicted demand, D_t^P , that aims to maintain enough stored energy in the FESS when the transformer operates close to its maximum limit. This amount of stored energy can be utilized by the SC controller to prevent direct power flow violations due to demand prediction uncertainty. We define \underline{C}_t^d as

$$\underline{C}_t^d = \begin{cases} 0, & \text{if } D_t^P \leq \eta \bar{P}^F, \\ \frac{\mu}{(1-\eta)\bar{P}^F} (D_t^P - \eta \bar{P}^F), & \text{if } \eta \bar{P}^F \leq D_t^P \leq \bar{P}^F, \\ \mu, & \text{otherwise.} \end{cases} \quad (13)$$

Notice that $\underline{C}_t^d = 0$ when the predicted demand is small, $D_t^P \leq \eta \bar{P}^F$, to avoid unnecessary FESS energy losses; further increase of the predicted demand increases linearly \underline{C}_t^d , until a maximum value μ is reached. The specific definition of \underline{C}_t^d creates a desirable region of the FESS SoC, as shown in Fig. 4. Hence, Problem \mathbb{P}_U aims to manage demand prediction uncertainty by minimizing the total SoC energy violations, yielding the formulation:

$$\min_{\mathbf{w}} f_U(\mathbf{w}) = \sum_{t \in \mathcal{T}} w_t \Delta T \quad (\mathbb{P}_U) \quad (14a)$$

$$\text{s.t. Constraints (4b)-(4c), (4e)-(4g),} \quad (14b)$$

$$(8a)-(8d), (11c), \quad (14c)$$

$$0 \leq x_t \leq x_t^E, \quad \forall t \in \mathcal{T}. \quad (14d)$$

In Problem \mathbb{P}_U , x_t^E denotes the optimal values of variables $x_t, \forall t \in \mathcal{T}$ obtained from the solution of Problem \mathbb{P}_E .

Finally, Problem \mathbb{P}_L aims to achieve economic efficiency for the FESS by minimizing its total energy losses while ensuring minimum transformer power violations and minimum total SoC energy violations:

$$\min_{\mathbf{P}^L} f_L(\mathbf{P}^L) = \sum_{t \in \mathcal{T}} P_t^L \Delta T \quad (\mathbb{P}_L) \quad (15a)$$

$$\text{s.t. Constraints (4b)-(4c), (4e)-(4g),} \quad (15b)$$

$$(8a)-(8d), (11c), (14d), \quad (15c)$$

$$0 \leq w_t \leq w_t^*, \quad \forall t \in \mathcal{T}. \quad (15d)$$

In Problem \mathbb{P}_L , w_t^* denotes the optimal values of variables $w_t, \forall t \in \mathcal{T}$ obtained from the solution of Problem \mathbb{P}_U .

In sum, every T_{MPC} the MPC controller sequentially solves Problems \mathbb{P}_V , \mathbb{P}_E , \mathbb{P}_U , and \mathbb{P}_L . All four problems can be fast and reliably solved using linear programming.

C. Secondary Controller

Algorithm 1 describes the operation of the SC controller that compensates the transformer power limit violations by

Algorithm 1 : FESS power set-point correction every 30 s

```

1: Input:  $P^S$ ,  $P^F$  and  $\hat{D}^A$ .
2: if  $(\hat{D}^A - P^S) > \max(P^F, \bar{P}^F)$  then
3:   Set  $P^R = \hat{D}^A - \max(P^F, \bar{P}^F)$ ;
4: else if  $(\hat{D}^A - P^S) < \min(P^F, \underline{P}^F)$  then
5:   Set  $P^R = \hat{D}^A - \min(P^F, \underline{P}^F)$ ;
6: else
7:   Set  $P^R = P^S$ ;
8: end if
9: Output:  $P^R$ .

```

handling the load uncertainty. This controller takes as input the FESS power set point, P^S , and transformer operating power, P^F , predicted from the MPC controller for the current 3-minute time cycle, as well as the latest measurement of the actual net load \hat{D}^A . The aim of the SC controller is to operate the transformer between the minimum and maximum permissible power points defined as $\min(P^F, \underline{P}^F)$ and $\max(P^F, \bar{P}^F)$, respectively. Hence, the SC controller provides a revised FESS power set-point P^R every T_{SC} s by considering three cases:

- 1) The transformer is set to operate at the maximum permissible point if this point is violated considering the MPC-based set-points and the latest measured net load (Lines 2-3).
- 2) The transformer is set to operate at the minimum permissible point if this point is violated (Lines 4-5).
- 3) Otherwise, the FESS power set-point remains unaltered (Lines 6-7).

Note that the FESS power and energy limits are ensured by the embedded primary controller in the real FESS. In the simulations, the power and energy limits are ensured in the Plant by projecting¹ parameter P^R to its feasible set defined by Eqs. (4e) - (4g) and (7e).

VI. SIMULATION RESULTS

The simulation setup is comprised of a FESS installed in a transformer substation with direct and reverse power flow limits of 500 kW and -200 kW, respectively. For comparison purposes two FESSs are considered:

- The *scaled-up prototype FESS* is a 100-times scaled-up version of a real prototype FESS². The scaled-up prototype FESS has a rated capacity of 185 kWh and 600 kW charging/discharging power. Its power losses and maximum power coefficients are $\hat{b}^c = 0.106$, $\hat{c}^c = 0.394$, $\hat{b}^d = 0.223$, $\hat{c}^d = 0.419$, $\hat{\alpha} = 0.172$ and $\hat{\beta} = 0.622$. These coefficients correspond to the ones identified experimentally for the real prototype FESS in Section VII-B.
- The *commercial FESS* has the same rated capacity and maximum charging/discharging power with the scaled-up prototype FESS. Its power losses and maximum power coefficients are $\hat{b}^d = \hat{b}^c = 0.075$, $\hat{c}^d = \hat{c}^c = 0.2$, $\hat{\alpha} = 0.172$ and $\hat{\beta} = 0.622$. These power losses coefficients

¹The projection of point x_0 on a set \mathcal{C} , is defined as the point $x_P \in \mathcal{C}$ that is closest to x_0 according to some distance metric $\|\bullet\|$, i.e., $x_P = \operatorname{argmin}\{\|x - x_0\| \mid x \in \mathcal{C}\}$. For example, the projection of x_1 on the set $[\underline{x}, \bar{x}]$ is simply $x_P = \max(\underline{x}, \min(\bar{x}, x_1))$ [26].

²The real prototype FESS is employed in Section VII for experimental validation.

correspond to 85% round-trip efficiency and 20% standby losses per hour [3].

Unless otherwise stated, $N = 10$ segments are used for the piecewise linear approximation of the FESS maximum power of both FESSs, according to Eqs. (8c) - (8d).

Section VI-A investigates the performance of the proposed methodology in two 6-hour scenarios, $T = 6$ hours, where *Scenario 1* has no uncertainty, while *Scenario 2* has model and net load demand uncertainty. Section VI-B provides aggregate results on the capability of the proposed controllers to provide peak shaving services under net load demand uncertainty, using historical data from a real distribution grid. The time-horizon is set to $T = 24$ hours. The timing parameters of the control architecture for both sections are set to: $\Delta T = 3$ min, $T_{MPC} = 3$ min, $T_{SC} = 30$ s, $T_m = 5$ s, and $T_{ex} = 10$ s. The solution of Problem \mathbb{P}_{LEX} takes place in the interval [165, 175] s of each MPC control-step. The allowed 10-second interval for the solution of the MPC Problem \mathbb{P}_{LEX} is more than enough, as Problems \mathbb{P}_V , \mathbb{P}_E , \mathbb{P}_U , and \mathbb{P}_L are medium-scale linear programs. These problems are solved using Gurobi [27]. Note that the predicted demand is usually available for 15-minute time intervals [6]; however, this work considers $\Delta T = T_{MPC} = 3$ min to provide updated control actions in shorter times, because the model uncertainty and the SC operation can affect the FESS SoC.

A. Performance Evaluation - Synthetic Data

Scenario 1: This scenario investigates the capability of the proposed MPC controller to provide peak shaving services to the distribution grid. Because there is no uncertainty, the SC controller is not utilized in this scenario. Therefore, the control actions of the MPC controller are passed directly to the Plant, without revision by the SC controller (see Fig. 2). Regarding the minimum desirable SoC, it is set that $\mu = 15\%$ and $\eta = 70\%$.

Fig. 5(a) presents the net load demand and the transformer operation using the two FESSs. To induce reverse and direct power violations, the net load is selected to have excessive PV generation and low load demand during noon and the opposite during afternoon hours. The results illustrate that the MPC controller successfully shaves the power peaks to maintain operation within safety limits. In detail, the reverse power violations, observed during [0.5 h, 1.25 h], are eliminated by charging the two FESSs from the excess PV production, as can be seen in Fig. 5(b). Notice in Fig. 5(c) that the surplus energy stored and re-injected into the grid is larger for the commercial FESS because it has lower standby losses compared to the prototype FESS. Due to the standby losses, the stored energy during [0.5 h, 1.25 h] is not maintained to address direct power violations, observed during [4.75 h, 6 h]. However, direct power violations are eliminated by charging the two FESSs from the grid prior to the violation period and reusing the stored energy to satisfy the excess load demand. As expected, the SoC at $T = 6$ h is 15% due to the minimum desirable SoC.

We further consider a case where the transformer maximum limit is reduced from 500 to 470 kW such that the safety limits cannot be satisfied, considering only the scaled-up prototype

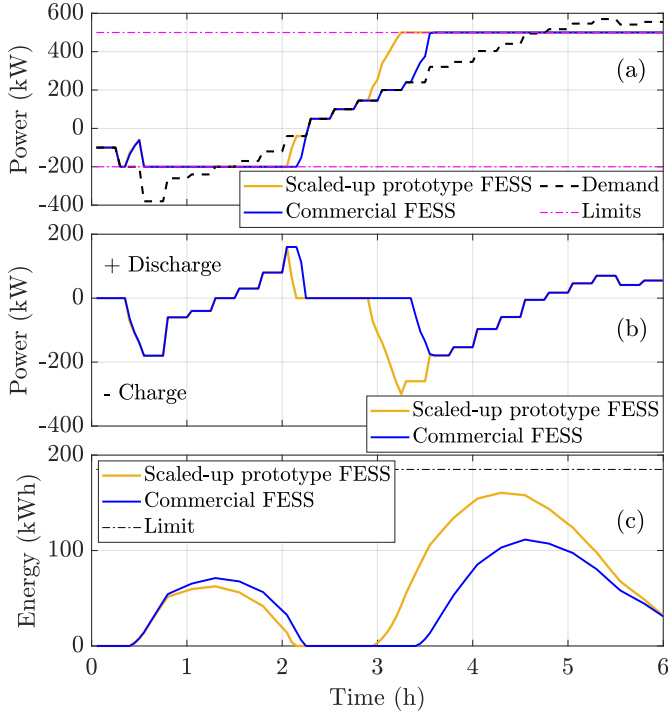


Fig. 5. Power scheduling using the scaled-up prototype and the commercial FESS: (a) Predicted net load demand and transformer power using the two FESSs, (b) FESS power set-points of the MPC controller, and (c) Stored energy in the prototype and commercial FESS.

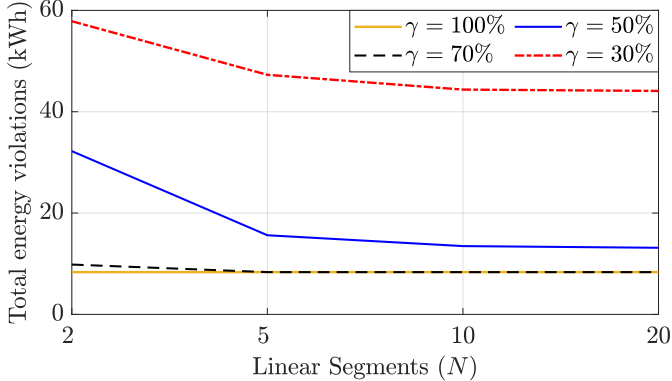


Fig. 6. Transformer energy violations for different number of segments, N , when the scaling factor γ is equal to 100%, 70%, 50% and 30%.

TABLE II

OBJECTIVES EFFECTIVENESS IN MINIMIZING POWER VIOLATIONS

Objectives	Peak power violation	Total energy violations
MinMax	4.1 kW	18.8 kWh
MinEnergy	85.1 kW	5.4 kWh
Lexicographic	4.1 kW	8.3 kWh

FESS. Table II presents the transformer peak violations and total energy violations under three objectives:

- 1) *MinMax* minimizes the transformer peak power violation as defined in Eq (11a).
- 2) *MinEnergy* minimizes the total energy violations as defined in Eq (12a).
- 3) *Lexicographic* combines the above two objectives and is defined as $\text{lexmin}\{f_V(\mathbf{x}), f_E(\mathbf{x})\}$.

From the results it is evident that the Lexicographic objective is the best as it achieves the smallest possible peak violation

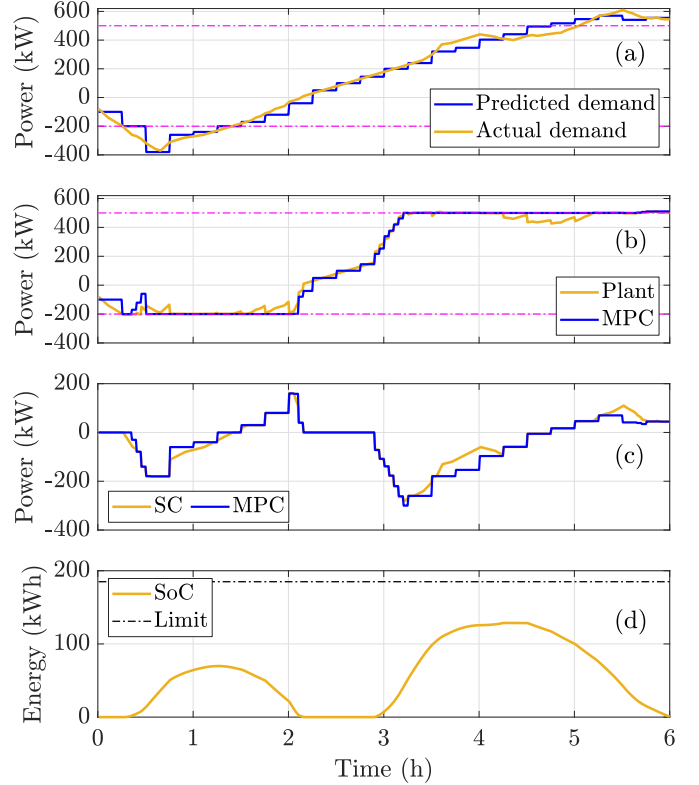


Fig. 7. Power scheduling using the scaled-up prototype FESS under uncertainty: (a) Actual and predicted net load demand, (b) Actual (Plant) and predicted (MPC) transformer power, (c) FESS power set-points of the MPC and SC controllers, and (d) Stored energy in the FESS.

(4.1 kW or 0.8% overloading) with only a small increase in the transformer total energy violations (2.9 kWh).

The *Lexicographic* objective is also used to investigate the impact of the piecewise linear approximation of Eq. (7e) on the total energy violations when the transformer maximum limit is 470 kW. As shown by the solid orange line of Fig. 6, there is no impact of N on the total energy violations under the FESS maximum power is 600 kW ($\gamma = 100\%$). For this reason, we re-scale the FESS maximum power limits in Eqs. (4g) and (7e) by a scaling factor γ , yielding the new constraints

$$\begin{aligned} \gamma P_t^S &\leq P_t^S \leq \gamma \bar{P}^S, \quad \forall t \in \mathcal{T}, \\ |P_t^S| &\leq \gamma(\hat{\alpha} + \hat{\beta}\sqrt{C_t^S}), \quad \forall t \in \mathcal{T}, \end{aligned}$$

and examine the performance for $\gamma = \{70\%, 50\%, 30\%\}$. Interestingly, the energy violations are considerably, moderately and marginally reduced when N increases from 2 to 5, 5 to 10 and 10 to 20, respectively. Hereafter, it is considered in all experiments that $N = 10$.

Scenario 2: Scenario 2 extends the simulation setup of Scenario 1 for the scaled-up prototype FESS by considering model and net load demand uncertainty. As a result, both controllers are utilized; the MPC controller computes the FESS power set points using the predicted demand and estimated model, while the SC controller corrects the provided points based on real-time measurements. Modelling uncertainty is introduced by increasing the FESS power losses by +5%. To introduce demand uncertainty, the predicted demand is computed as the 15-minute piecewise constant approximation

of the actual demand; the mean, standard deviation, minimum and maximum demand prediction error is 1.5 kW, 38.6 kW, -91.7 kW and 115 kW, respectively.

Fig. 7(a) illustrates the actual and predicted demand and Fig. 7(b) presents the actual and predicted transformer power, produced by the Plant and the MPC controller. Despite the introduced uncertainty, the proposed controllers can still handle well the reverse and direct power violations. This is also indicated in Fig. 7(c) by the revised FESS power set-points of the SC controller which correct the set-points of the MPC controller. The minimum desirable SoC is vital in making these corrections; for example, the unpredicted extra demand experienced in the period [5h, 6h] is compensated using the FESS minimum desirable SoC, resulting in almost 0% SoC at the end of the 6-hour scenario.

B. Performance Evaluation - Real Data

This section examines the capability of the proposed controllers to provide peak shaving services under net load demand uncertainty, using historical data from a real distribution substation in Larnaca, Cyprus. Fig. 8 demonstrates 31 actual net load curves that are obtained from the distribution transformer for July 2019, as provided by the Cyprus Distribution System Operator (DSO). It also presents a predicted net load curve constructed as the average of the actual net load curves of July 2018. The distribution grid includes mainly residential loads of a rural area and there is intense penetration of large PV parks, causing high reverse and direct power flows during the noon and evening hours, respectively, as can be seen in Fig. 8. As power violations do not occur in the real distribution transformer, due to its large size, we consider a smaller transformer with peak reverse and direct capability of -200 kW and 500 kW. The performance of the proposed controllers is examined for the commercial FESS using as input the actual and predicted net load curves of Fig. 8 for the Plant and the MPC, respectively, according to Fig. 2.

Figs. 9 (a) and (b) illustrate the energy violations of the 31 actual curves, in box-plot form³, that are caused due to the direct and reverse power flow violations, when no control and MPC control are used, respectively. Although MPC control achieves better results compared to no control, it still suffers from high energy violations because only the “expected” violations that are covered by the predicted net load curve are addressed. Note that the values of μ and η do not affect the energy violations, because the SC controller is deactivated.

When both the MPC and SC controllers are utilized, the reverse energy violations are completely eliminated because the SC controller stores all the “unexpected” violated energy in the FESS. Nevertheless, the “unexpected” violated energy from the direct power flow is more challenging to be addressed, because the FESS must be charged in advance to provide the violated energy. Fig. 10 presents the direct energy violations of the actual curves for different values of

³The bottom and top of each box indicate the first and third quartiles (25% and 75%) of a ranked data set, while the horizontal line inside the box indicates the median value (second quartile). The horizontal lines outside the box indicate the lowest/highest datum still within 1.5 inter-quartile range of the lower/upper quartile; for normally distributed data this corresponds to approximately 0.35%/99.65%.

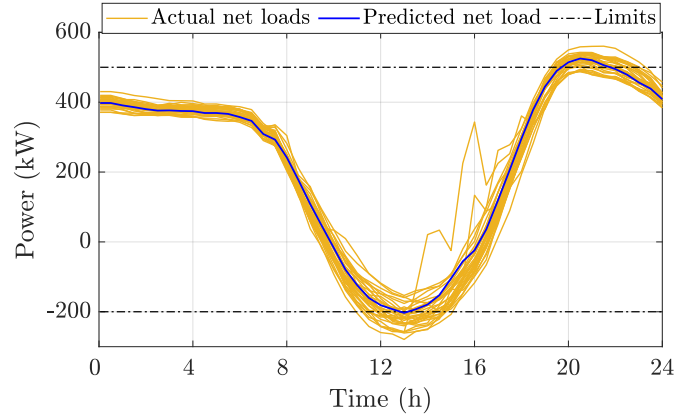


Fig. 8. Actual and predicted net load curves constructed from historical data of a real distribution grid.

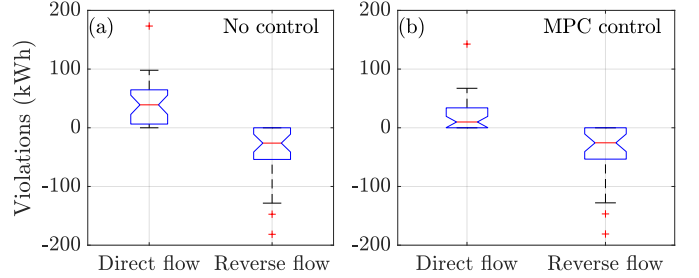


Fig. 9. Direct and reverse energy violations when (a) the proposed control scheme is not utilized and (b) the MPC controller is used, but the secondary controller is deactivated.

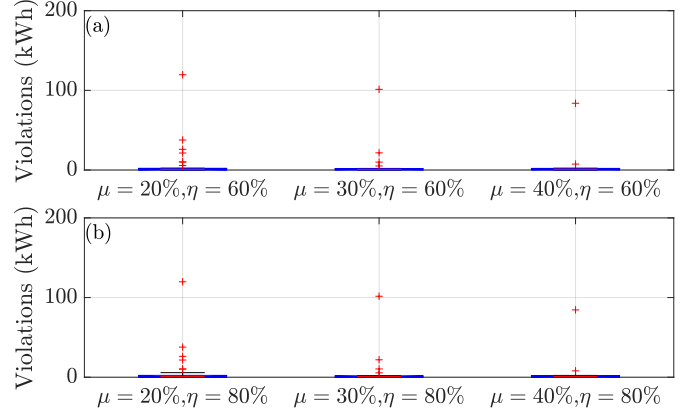


Fig. 10. Direct energy violations, in box-plot form, for different μ and η when both the MPC and secondary controllers are utilized. The reverse energy violations are eliminated in every case.

μ and η (see Eq. (13)). As expected, the energy violations are reduced as the value of μ increases, because more energy is maintained in the FESS to address the “unexpected” violations. In contrast, parameter η has negligible effect on the results; nonetheless, higher values of η are more preferable to avoid unnecessary power losses due to the FESS operation. As shown in Fig. 10, the proposed controllers compensate well for the “unexpected” energy violations of the considered days for $\mu = 40\%$. However, high energy violations are still present in one particular day with total energy violations of 173.3 kWh (see the Direct flow in Fig. 9 (a)). This amount of energy cannot be compensated by the considered FESS with capacity 185 kWh, efficiency 85% and standby losses 20%. The main conclusions of this section are summarized as:

- 1) In cases with high net load uncertainty, the utilization of

both the MPC and SC controllers is essential to address the “unexpected” power and energy violations.

- 2) The violations are reduced by increasing parameter μ ; η has negligible effect on the results.
- 3) The FESS capacity is an important factor that affects the performance of the proposed controllers, since small values impose energy limitations that can lead to transformer power limit violations.

VII. EXPERIMENTAL VALIDATION

In this section, the proposed controllers are evaluated in a realistic experimental setup using a real prototype FESS. Prior to the performance evaluation, the experimental setup is described and used to identify the parameters of the power losses and maximum power FESS functions.

A. Experimental Setup

As shown in Fig. 11, the experimental setup is comprised of five main modules: (M1) the Physical System, (M2) the Core Context Management, (M3) the Communication Context, (M4) the Processing Context, and (M5) the Visualization Context. The *Physical System* represents the considered smart-grid configuration presented in Fig. 1. It is comprised of a prototype FESS with 6 kW total rated power and a usable capacity of 1.85 kWh, a 4.05 kW load bank with nine equal controllable switching steps and a 5 kW PV system, connected to the power grid and installed in our power systems laboratory. The FESS is based on two 150 kg flywheels with a rated speed of 14000 RPM and the PV system is based on a commercial Fronius Symo 5.0 inverter associated with a Chroma 62150H PV emulator. Measurements of the various system states (actual load, grid power) are obtained through smart meters while the PV generation and the FESS charging/discharging power and SoC are obtained through the inverter and FESS interfaces.

To enable the interaction between the controllers and the physical system, a software platform based on FIWARE [17] has been developed (modules M2 - M5). FIWARE is a framework of an open source platform modules which can be assembled together to accelerate the development of smart solutions, such as the real-time monitoring and control of a FESS in a smart grid environment. In the developed FIWARE-based software platform, the *Core Context Management* module is responsible for creating and managing context information elements through the Orion Context Broker sub-module, as well as storing, querying and retrieving data using Quantum-Leap from the back-end database (CrateDB). The exchange of information between the Core Context Management and the Physical System is achieved through the *Communication Context* module where a Python script has been developed to transfer real-time measurements from the smart meters to the Core Context Management. Measurements are submitted to the Processing Context module and are displayed graphically on the *Visualization Context* (developed using Grafana web application) to monitor the system. The *Processing Context* module implements the proposed controllers in Matlab/Gurobi and calculates the FESS commands which are submitted for execution to the Physical System through a C# script. Measurement and control data between the Physical System

TABLE III
REGRESSION ANALYSIS - PARAMETER IDENTIFICATION

Charg. mode - Eq. (7c)	Disch. mode - Eq. (7b)	Max. power - Eq. (7e)
$\hat{b}^c = 0.106, \hat{c}^c = 0.394$	$\hat{b}^d = 0.223, \hat{c}^d = 0.419$	$\hat{\alpha} = 0.172, \hat{\beta} = 0.622$
Adjusted $R^2 = 0.973$	Adjusted $R^2 = 0.961$	Adjusted $R^2 = 0.996$
RMSE = 0.046	RMSE = 0.103	RMSE = 0.081

and the Core Context Management are exchanged through the laboratory Local Area Network (LAN). Note that the experimental setup operates according to the three different time scales presented in Fig. 3.

B. FESS Model Validation and Parameter Identification

This section validates the proposed model for the power losses, Eqs. (8a)-(8b), and maximum power, Eqs. (8c)-(8d), of the employed prototype FESS. To derive the charging power losses, the FESS operation was regulated with a constant charging power for varying SoC and maximum allowable power. The power losses were then calculated at each operating condition pairs (SoC, charging power) as the difference between the measured absorbed energy for charging and the measured stored energy in the FESS. For example, the power losses at 50% SoC and 2 kW charging power are derived by the difference between the energy drawn from the grid and the FESS stored energy for a SoC increase from 45% to 55% using a constant charging power of 2 kW. A similar approach was used for the discharging mode.

The FESS power losses as a function of the charging/discharging power and the SoC are illustrated in Fig. 12. From the figure two important observations can be made. First, the FESS power losses become higher as the charging/discharging power and the SoC increase. Second, the maximum power depends on the SoC, as shown in Fig. 13, and thus the measurements on the power losses do not span the entire SoC/maximum power region. Due to this limitation, the total number of measurements were 166 instead of 225 when the SoC and maximum power vary in the ranges $\{10, 20, \dots, 90\%$ and $\{-6, -5.5, \dots, 5.5, 6$ kW}, respectively. The maximum charging/discharging power limitation is further verified according to experimental measurements received from the FESS interface, as shown in Fig. 13, which indicates that the maximum power is a monotonically increasing concave function of the SoC.

Linear regression was used to model the FESS power losses (kW) as a function of the SoC (kWh) and the charging or discharging rate (kW). Table III presents the identified parameters of the two linear models for the charging and discharging modes, according to Eqs. (7b)-(7c) or Eqs. (8a)-(8b), along with two coefficients to determine the goodness of fit. The *Adjusted Coefficient of Determination* (Adjusted R^2) falls very close to 1 (Adjusted $R^2 > 0.95$) in both cases; this indicates that the derived models explain more than 95% of the variance in the power losses. The goodness of fit is also indicated by the small *Root Mean Squared Error* (RMSE) values which are less than 0.105 kW in both cases.

The results of the linear regression are illustrated in Fig. 12 by the two intersecting planes representing the power losses for the charging and discharging mode. As can be seen, the two

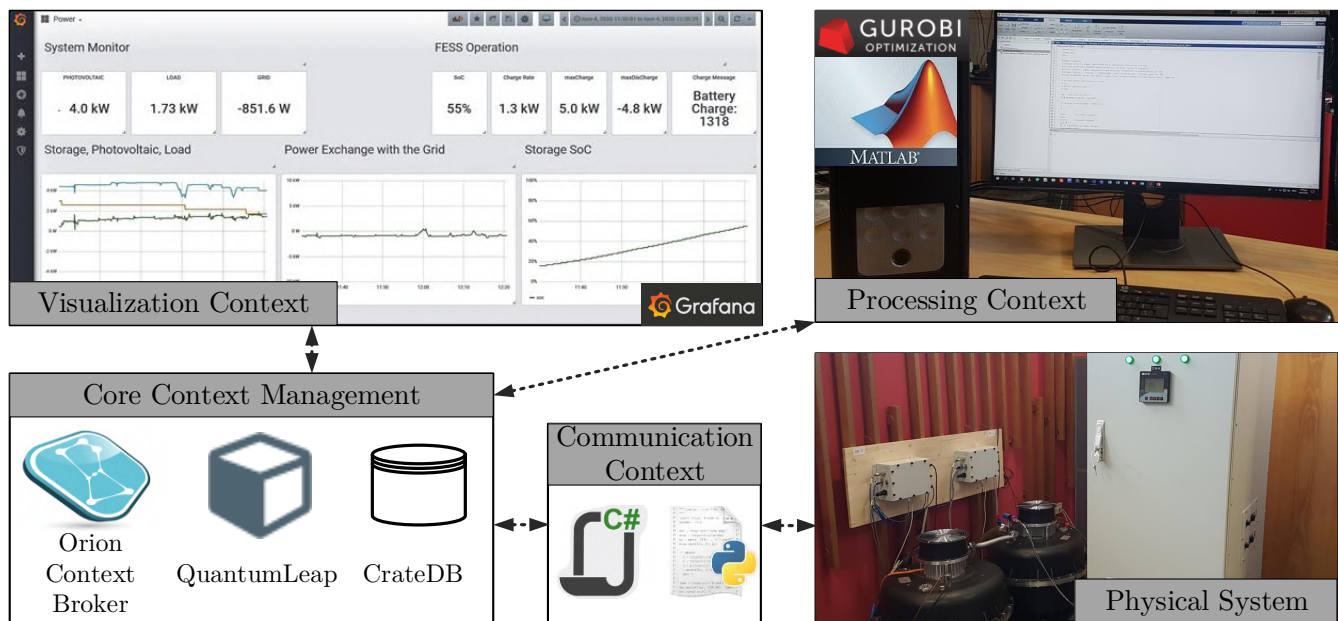


Fig. 11. Monitoring and control of the FESS for providing distribution grid services using a software platform based on FIWARE.

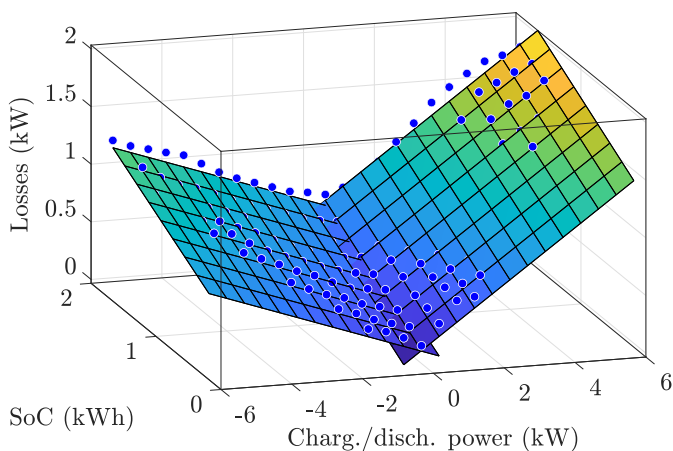


Fig. 12. The FESS power losses for varying SoC and charging/discharging power. The two intersecting planes is the result from linear regression using the sample points and the dots indicate sample points located above the planes.

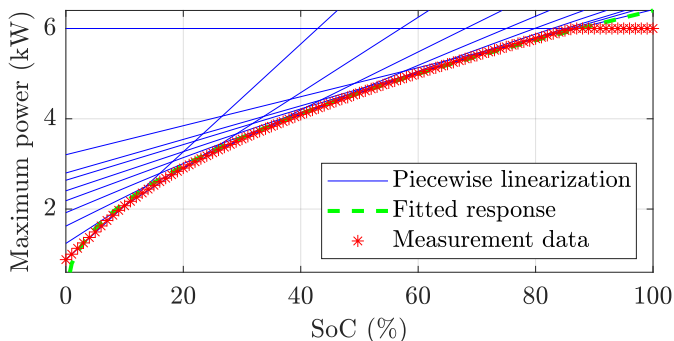


Fig. 13. The maximum charging/discharging power of the FESS as a function of the SoC obtained from 100 experimental samples. The dashed line is the fitted response using regression. The ten blue solid lines construct a piecewise linear approximation of the concave function produced from the samples.

intersecting planes define a convex function which explains the selection of Eqs. (8a)-(8b).

Similarly, the parameters of the maximum power model, Eq. (7e), are identified using linear regression based on the

measurements depicted in Fig. 13. Table III shows an excellent goodness of fit having an Adjusted R^2 value larger than 0.99 and a RMSE smaller than 0.01 kW. The fitted model and a 10-segment piecewise linear approximation of the model are shown in Fig. 13. These linear segments are used to derive convex constraints on the maximum power in (8c)-(8d).

C. Experimental Results

To experimentally evaluate the two proposed controllers, we consider a 3-hour scenario, $T = 3$ hours, with power grid limits of 3.3 kW and -1 kW and the experimental setup described in Section VII-A. The timing parameters used in Section VI for the control architecture remain the same. Fig. 14(a) shows the PV generation and load demand of the physical system, as well as actual and predicted net load demand. Fig. 14(b) illustrates that the controllers successfully shave the peaks exceeding the power limits in almost all cases. Fig. 14(c) presents the FESS power set-points of the MPC and SC controllers. As can be seen, major deviations between the controllers output are experienced during the period [0h, 1h]; however, the SC controller manages to successfully compensate the unpredicted extra net load demand and maintain the power grid limits. Finally, the FESS SoC due to the charging/discharging power is illustrated in Fig. 14(d).

VIII. PRACTICAL IMPLEMENTATION CONSIDERATIONS

The practical implementation of the proposed energy management and control scheme for providing peak shaving services requires proper consideration of (a) the transformer power limit violations, (b) the cost-effective operation of the system, and (c) communication and cybersecurity issues.

The size (capacity) of the FESS is a key aspect that can lead to violations of the transformer power limit. As presented in Section VI-B, a small FESS imposes energy limits and violations can occur. Thus, before the investment, a planning study must be carried out, considering the historical and future power

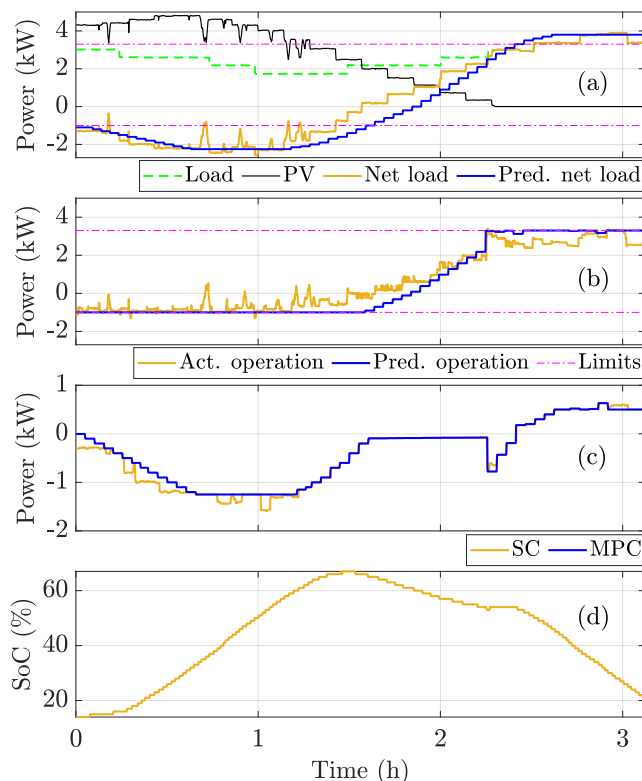


Fig. 14. Experimental validation using the prototype FESS: (a) Input data, (b) Actual (Plant) and predicted (MPC) transformer operation, (c) FESS charging/discharging power based on the MPC and SC controllers, and (d) SoC.

profiles of the transformer, to determine the adequate size of the FESS for each application. In addition, the utilization of an accurate predicted curve for the transformer net load is required to enhance the performance of the proposed scheme. This predicted curve can be constructed using forecasting data and/or historical data, as indicated in Section VI-B. In case the proposed scheme fails to eliminate all violations, PV curtailments and/or load shedding must be applied to avoid overloading the distribution transformer.

The FESS efficiency and standby losses is an important factor that should be considered for the cost-effective operation of the system in real applications. Low efficiency and high standby losses result in significant total energy losses that affect the sustainability of the investment. In addition, high energy losses affect the FESS mission profile (charging/discharging power) resulting in higher power rates which can affect the lifetime of the FESS power electronics, especially when the system operates near to its rate limits [28]. Such a case was illustrated in Fig. 5, where the prototype FESS resulted in significantly higher charging power compared to the more efficient commercial FESS.

Secure communication is also a major concern in smart grid applications. In this work, measurement and control data between the Core Context Management and the Physical System are exchanged through a LAN, since all modules of the experimental setup, presented in Fig. 11, were located within the same building. However, in real-world applications, the physical systems may be distributed far away from the central Monitoring and Processing Contexts (server or cloud-based). In this case, secure and reliable communication can

be achieved over the Internet using different methods. Two indicative approaches are the following. The first approach is to use a Virtual Private Network (VPN) router at the physical system level to facilitate secure communication with a central processing server. The second approach is to use a local controller with firewall protection to maintain communication between the components at the physical level through a LAN. In the latter case, only the local controller can communicate over the Internet with the central Processing Context in a bi-directional way using secure Internet of Things (IoT) protocols such as the Message Queuing Telemetry Transport (MQTT) protocol.

IX. CONCLUSIONS

In this work, an energy management and control scheme is proposed to provide peak shaving services to the distribution grid using a FESS. Convex functions that represent the FESS power losses and maximum power are derived and incorporated in a novel lexicographic optimization that defines the FESS power set-points. A two-level hierarchical control scheme is proposed for the solution of the lexicographic optimization to deal with demand prediction errors and modelling uncertainty. In this study the proposed FESS modelling is experimentally validated and the FESS parameters are identified. Simulation and experimental results validate the effectiveness of the proposed energy management and control scheme to provide peak shaving services under realistic conditions. The proposed scheme enables the active management of distribution grids and increases the hosting capacity for PV installations and load demand growth in existing power grids.

REFERENCES

- [1] S. Nykamp et al., "Value of storage in distribution grids—competition or cooperation of stakeholders?," in *IEEE Trans. Smart Grid*, vol. 4, no. 3, pp. 1361-1370, Sept. 2013.
- [2] M. H. Pandya et al., "Enhancing the distribution feeder capacity through energy storage," in *Proc. IEEE ICIT*, Cape Town, 2013, pp. 1739-1744.
- [3] F. Nadeem et al., "Comparative review of energy storage systems, their roles, and impacts on future power systems," in *IEEE Access*, vol. 7, pp. 4555-4585, 2019.
- [4] Y. Yang et al., "Cost-benefit study of dispersed battery storage to increase penetration of photovoltaic systems on distribution feeders," in *Proc. IEEE PES General Meeting*, National Harbor, MD, 2014, pp. 1-5.
- [5] T. Zhang, A. E. Emanuel and J. A. Orr, "Distribution feeder upgrade deferral through use of energy storage systems," in *Proc. IEEE PES General Meeting*, Boston, MA, 2016, pp. 1-5.
- [6] D. Kodaira, W. Jung and S. Han, "Optimal energy storage system operation for peak reduction in a distribution network using a prediction interval," in *IEEE Trans. Smart Grid*, Oct. 2019.
- [7] J. Tant, F. Geth, D. Six, P. Tant and J. Driesen, "Multiobjective battery storage to improve PV integration in residential distribution grids," *IEEE Trans. Sustain. Energy*, vol. 4, no. 1, pp. 182-191, Jan. 2013.
- [8] Z. Taylor et al., "Battery-assisted distribution feeder peak load reduction: Stochastic optimization and utility-scale implementation," in *Proc. IEEE PES General Meeting*, Boston, MA, 2016, pp. 1-5.
- [9] Z. Taylor et al., "Customer-side SCADA-assisted large battery operation optimization for distribution feeder peak load shaving," in *IEEE Trans. Smart Grid*, vol. 10, no. 1, pp. 992-1004, Jan. 2019.
- [10] A. Nagarajan and R. Ayyanar, "Design and strategy for the deployment of energy storage systems in a distribution feeder with penetration of renewable resources," in *IEEE Trans. Sustain. Energy*, vol. 6, no. 3, pp. 1085-1092, July 2015.
- [11] L. Tziouvani, P. Kolios, L. Hadjidemetriou and E. Kyriakides, "Grid friendly operation of a PV-storage system with profit maximization and reliability enhancement," in *Proc. IEEE SEST*, Porto, 2019, pp. 1-6.
- [12] G. Parise et al., "Comprehensive peak-shaving solutions for port cranes," in *IEEE Trans. Industry Appl.*, vol. 53, no. 3, pp. 1799-1806, 2017.

- [13] G. O. Suvire et al., "Improving the integration of wind power generation into AC microgrids using flywheel energy storage," in *IEEE Trans. Smart Grid*, vol. 3, no. 4, pp. 1945-1954, Dec. 2012.
- [14] F. Islam, A. Al-Durra and S. M. Mueeen "Smoothing of wind farm output by prediction and supervisory-control-unit-based FESS," in *IEEE Trans. Sustain. Energy*, vol. 4, no. 4, pp. 925-933, Oct. 2013.
- [15] F. Díaz-González et al., "Energy management of flywheel-based energy storage device for wind power smoothing," in *Applied Energy*, vol. 110, pp. 207-219, Oct. 2013.
- [16] H. H. Abdeltawab et al., "Robust energy management of a hybrid wind and flywheel energy storage system considering flywheel power losses minimization and grid-code constraints," in *IEEE Trans. Industrial Electronics*, vol. 63, no. 7, pp. 4242-4254, July 2016.
- [17] FIWARE, 2020. [Online]. Available: "https://www.fiware.org".
- [18] H. Isermann, "Linear lexicographic optimization," *OR Spektrum* 4, pp. 223-228, 1982.
- [19] S. T. Gurumurthy et al., "Apportioning and mitigation of losses in a flywheel energy storage system," *Proc. IEEE PEDG*, Rogers, 2013, pp. 1-6.
- [20] C. S. Hearn et al., "Utilization of optimal control law to size grid-level flywheel energy storage," in *IEEE Trans. Sustain. Energy*, vol. 4, no. 3, pp. 611-618, July 2013.
- [21] C. Shi et al., "Charging-discharging control strategy for a flywheel array energy storage system based on the equal incremental principle," in *Energies Open Access Journal*, vol. 12, pp. 1-27, July 2019.
- [22] A. Soomro et al., "Performance and loss analysis of squirrel cage induction machine based flywheel energy storage system," in *Applied Sciences*, vol. 9, no. 21: 4537, Oct. 2019.
- [23] L. Mears et al., "EPRI-DOE Handbook of Energy Storage for Transmission and Distribution Applications," *Electric Power Research Institute; U.S Department of Energy*, Washington, DC, USA, 2003.
- [24] X. Chang et al., "Active Disturbance Rejection Control for a Flywheel Energy Storage System," in *IEEE Trans. Industrial Electronics*, vol. 62, no. 2, pp. 991-1001, Feb. 2015.
- [25] C. Sourkounis, "Storage system management for power conditioning in wind parks," *Proc. IEEE ENERGYCON*, Cavtat, Croatia, 2014, pp. 597-602.
- [26] S. Boyd and L. Vandenberghe, "Convex optimization," *Cambridge university press*, 2014.
- [27] Gurobi Optimization, LLC, "Gurobi Optimizer Reference Manual," 2020. [Online]. Available: "http://www.gurobi.com".
- [28] Y. Yang, H. Wang, F. Blaabjerg and T. Kerekes, "A hybrid power control concept for PV inverters with reduced thermal loading," in *IEEE Trans. Power Electronics*, vol. 29, no. 12, pp. 6271-6275, Dec. 2014.

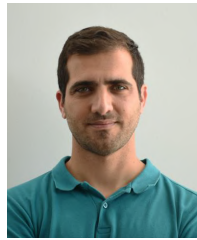


Lysandros Tziouvani (Student Member, IEEE) received the B.Sc. and M.Sc. Degrees in Electrical Engineering from the University of Cyprus, Nicosia, Cyprus, in 2015 and 2017, respectively. He is currently a Ph.D. candidate in the Department of Electrical and Computer Engineering at the University of Cyprus and a Researcher at KIOS Research and Innovation Center of Excellence. His research interests lie in the area of electric power systems, power system operation and optimization.



Lenos Hadjidemetriou (Member, IEEE) received the Diploma in Electrical and Computer Engineering in 2010 from the National Technical University of Athens, Athens, Greece, and his Ph.D. degree in Electrical Engineering in 2016 from the University of Cyprus. He is currently a Research Lecturer at the KIOS Research and Innovation Center of Excellence, University of Cyprus, Cyprus. His research interests include renewable energy systems, energy storage systems, control of power electronics, ancillary services, smart grids and microgrids. Dr.

Hadjidemetriou has published more than 75 papers in scientific journals and international conference proceedings. He has extensive experience on managing research projects in the area of smart grids and he has developed 3 advanced research laboratories in the University of Cyprus premises. Dr. Hadjidemetriou is a member of the Cyprus Technical Chamber. He volunteered as a reviewer to several IEEE transactions and conferences and received the best paper award in the power quality session at IEEE IECON13.



maintenance and inventory management for laboratory equipment.

Charalampos Charalampous received the BSc degree in 2012 and his MSc degree in Electrical Engineering in 2014 from the Department of Electrical and Computer Engineering at the University of Cyprus. His professional experience is related to the design and implementation of low voltage power systems. He joined KIOS Research and Innovation of Excellence in October 2017, where he is currently a Laboratory Manager and Research Engineer. His duties include, the design, implementation and maintenance of power systems experiments, purchase, maintenance and inventory management for laboratory equipment.



Maria Tziakouri received her B.Sc. degree in Computer Engineering from the Department of Electrical and Computer Engineering at University of Cyprus in 2015. In 2017, she received her M.Sc. degree in Computer Engineering from University of Cyprus. She is currently working as a Software Engineer at KIOS Research and Innovation Center of Excellence and she is involved in projects in the field of electric power systems and transportation systems.



Stelios Timotheou (Senior Member, IEEE) is an Assistant Professor at the Department of Electrical and Computer Engineering and a faculty member at the KIOS Research and Innovation Center of Excellence of the University of Cyprus. He holds a Dipl.-Ing. in Electrical and Computer Engineering (Summa Cum Laude, 2005) from the National Technical University of Athens, an MSc in Communications and Signal Processing (Distinction, 2006) and a PhD in Intelligent Systems and Networks (2010), both from the Department of Electrical and Electronic Engineering of Imperial College London. In previous appointments, he was a Research Associate at KIOS, a Visiting Lecturer at the Department of Electrical and Computer Engineering of the University of Cyprus, and a Postdoctoral Researcher at the Computer Laboratory of the University of Cambridge. His research focuses on monitoring, control and optimization of critical infrastructure systems, with emphasis on intelligent transportation systems, communication systems and power systems. He is the recipient of the 2017 Cyprus Young Researcher in Physical Sciences & Engineering Award, by the Cyprus Research Promotion Foundation.



Elias Kyriakides (Senior Member, IEEE) received the B.Sc. degree from the Illinois Institute of Technology, Chicago, IL, USA, in 2000, and the M.Sc. and Ph.D. degrees from Arizona State University, Tempe, AZ, USA, in 2001 and 2003, respectively, all in electrical engineering. He was an Associate Professor with the Department of Electrical and Computer Engineering, University of Cyprus, Nicosia, Cyprus, and a founding Member of the KIOS Research and Innovation Center of Excellence, University of Cyprus. His research interests included wide area monitoring and control of power systems, the optimization of power system operation techniques, and the integration of renewable energy sources. He served as the Action Chair of the ESF-COST Action IC0806 "Intelligent Monitoring, Control, and Security of Critical Infrastructure Systems" from 2009 to 2013. He was an Associate Editor of the IEEE Systems Journal and an Editor of the IEEE Transactions on Sustainable Energy.